Generalized active power flow controller for multi active bridge DC-DC converters with minimum-current-point-tracking algorithm

Hebala, Osama M.; Aboushady, Ahmed A.; Ahmed, Khaled H.; Abdelsalam, Ibrahim

Published in:
IEEE Transactions on Industrial Electronics

DOI:
10.1109/TIE.2021.3071681

Publication date:
2021

Document Version
Author accepted manuscript

Generalized Active Power Flow Controller for Multi Active Bridge DC-DC Converters with Minimum-Current-Point-Tracking Algorithm

Osama M. Hebala, Ahmed A. Aboushady, *Senior Member, IEEE*, Khaled H. Ahmed, *Senior Member, IEEE*, and Ibrahim Abdelsalam

***Abstract*— This paper proposes a new active power flow controller for DC-DC multi active bridge (MAB) converters with minimum current point tracking (MCPT) to minimize conductive losses. Unlike recent efforts in this area, the proposed controller does not require look-up table for implementation nor complex non-linear converter modelling and is not circuit parameter-dependent. The proposed control scheme is also generalized for MAB converters with any number of ports and is derived in per unit form to enable standard implementation for buck/boost/unity-gain operating modes. The proposed MCPT algorithm is based on an innovative adaptive perturb and observe (P&O) tracking of the minimum current point (MCP) on the MAB converter current characteristic plane. This MCP is tracked while active power regulation is simultaneously achieved based on a new phase shift decoupler to enable direct regulation of individual port active power. Detailed design procedure of the proposed controller is presented and extensive simulation is carried out to validate the effectiveness of the proposed MCPT closed loop controller. Experimental implementation is also provided to substantiate the simulation results.**

Index Terms*— DC-DC, Minimum current point tracking (MCPT), Multi Active Bridge (MAB), Perturb and Observe (P&O).

I. INTRODUCTION

MULTI active bridge (MAB) converters have lately gained the attention of researchers as a potential solution for the renewables integration [1]–[5]. MAB is a family of multi-port DC-DC converters which has been proposed by [6]. It is a generic converter that can comprise any number of active bridges (H-bridge) to increase the a number of power ports [7]. The main driver for developing MAB converters is the need of technology that enables integrating of distributed generation and storage into the distribution networks. Their main advantages are interconnection of several sources with different voltage ratings via a single high frequency transformer with adjustable turn ratios, zero-voltage switching (ZVS) capability and reduced DC-DC conversion stages, which yields a higher power density[4][8][9].

Moreover utilising MAB converter can offer integrated control design with reduced number of controllers needed in multiple-stage configurations based on dual-active-bridge (DAB) [10], which ensures more stability and eliminates the need to study the interaction between controllers[4]. In addition, MAB offers cascaded or modular configuration capability in case of higher power/voltage requirements. On the other hand, when number of H-bridges increases, control schemes become very complicated to be designed and implemented. As an example, there are 256 switching states in a quad active bridge converter [7]. In fact, with presence of such a high number of states, the normally used piecewise linear control methods do not provide sufficient insight into the converter operation.

Control scheme design for MAB converters has been an active research topic since many years. The main research areas are performance optimization and decoupling control design, which is vital in terms of dealing with the nonlinearity and high coupling of powers and phase shifts in MAB converters [11]. In [1], power flow decoupling controller has been explored for a triple active bridge (TAB) converter, which comprises different ports of sources and loads. A closed loop control was developed for a dual transformer TAB in [2], however coupling via multiple transformers usually leads to higher cost and lower power density. A decupling power flow management schemes for a quad active bridge (QAB) were proposed in [3] for traction application, in [4] for integration of distributed generation/storage and in [5] for Aircraft network. Decoupling control for a QAB converter has been also studied in [12] with a focus on the transformer design and efforts to manipulate duty ratios to achieve better efficiency.

This Manuscript received Aug 02,2020; revised Sep 9, 2020 and Nov 24, 2020 and Feb 5,2021; accepted Mar 24, 2021.

O. M. Hebala is with Electrical and Control Engineering Department, Arab Academy for Science and Technology and Maritime Transport, Alexandria 1029, Egypt (e-mail: ohibala@aast.edu).

A. A. Aboushady is with the School of Computing, Engineering and Built Environment, Glasgow Caledonian University, Glasgow G4 0BA, U.K (e-mail:ahmed.aboushady@ieee.org).

K. H. Ahmed is with the Department of Electronic and Electrical Engineering, University of Strathclyde, Glasgow G1 1XW, U.K, and the Department of Electrical Engineering, Faculty of Engineering, Alexandria University, Alexandria, Egypt (e-mail: khaled.ahmed@ieee.org).

I. Abdelsalam is with the Electrical Engineering Department, Arab Academy for Science and Technology and Maritime Transport, Cairo 1029, Egypt (e-mail: i.abdelsalam@aast.edu).

Reported control schemes in [1]–[5], [12] are not universal for *n*-port MAB converter. Besides, [1], [3]–[5] utilise fixed duty ratios, which leads to poor efficiency in light loads and/or DC voltage mismatch (i.e.: unmatched voltage amplitudes across the transformer sides.). In addition, [1] does not treat ports as sources/sinks of power enabling bi-directional power flow at any port. Generic modelling of n-port MAB is proposed in [7], besides an optimized controller based on Lagrange Multiplier. This involved some approximations to simplify and solve the highly complicated power transfer equations. This can cause inaccuracies and steady state errors in case any deviation between the model and the real value. In addition, Lagrange Multiplier lacks sufficiency as the optimization problem is non-convex. On the other hand,various control schemes have been proposed for MAB converter with only two ports (dual active bridge DAB), which is considered as the simplest form of MAB structure [13]–[16]. Predictive control and/or optimal TPS relations obtained by particle swarm optimization (PSO)/Lagrange Multiplier and/or utilizing look-up tables have been implemented in literature to operate DAB under most suitable (optimal) switching states to improve the converter efficiency. However, using similar control strategies extracted from two-port (DAB) converters for MAB with high number of H-bridges is very challenging and involves complicated modeling and/or requires a huge amount of data points.

From the discussion above, a common drawback can be concluded, which is the heavy dependency of controllers on complex converter modeling, non-linear equations and circuit parameters. In addition, scalability is overlooked, as control schemes are often case-specific with regard to either number of ports, voltage-power rating and/or unidirectional power flow assumption at certain ports. Additionally, there is a lack of an implement standard of multiple phase shifting in MAB converters. This leads to high current stresses and sub-optimum operation of converter, particularly: under light load or DC voltage mismatch. This explains the need of further advances in the modeling and control scheme design for MAB converters. This article proposes a universal solution that can be applied to active bridge converters with any number of DC ports tackling aforementioned challenges without compromising on control complexity and challenging real time implementation. In this context, this study puts forward a scalable bidirectional power flow controller that tracks minimum current in MAB converters. The focus of the controller is the minimization of copper and conduction losses. This is because conduction losses (per device) are dominant loss portion compared to switching losses in the widely used MOSFET power switches [17] [18]. Plus, conduction and copper losses are proportional to the square of the RMS current [15]. Like maximum power point tracking (MPPT) algorithms [19]–[23], a new adaptation of Perturb &Observer (P&O) tracking technique is used for the proposed control scheme. P&O algorithms do not necessitate former knowledge of the converter features and are straightforward in implementation. In this context, there are two major types of perturb calculations: fixed-step perturb [20],[21] and adaptive-step perturb [22], [23]. Since fixed-step perturb suffers from several drawbacks in steady state and the perturb value is not generic, this paper investigates a new adaptive-step P&O. The novel adaptive-step P&O utilizes rate of change of the converter's AC link RMS current by employing a simple PI controller for an adaptive perturb generation.

The paper is divided into seven sections. The basis for the proposed controller defining the DC-DC MAB converter I-V characteristic are provided in Section II. The proposed P&O minimum current point tracking (MCPT) algorithm is demonstrated in Section III. Subsequently, the complete closed loop controller design incorporating a new phase shift decoupler is stipulated in Section IV. As verification of the proposed controller performance, simulation and experimental results are presented in section V. Control performance evaluation is then presented in section VI, then followed by the concluding remarks in section VII.

II. MAB Converter I−V Characteristics

A. Phase shift modulation

An *n*-port MAB converter is comprised of *n* active-bridge modules magnetically coupled through an *n*-winding HF transformer as depicted in Fig. 1. The power flow between any two ports is essentially controlled through phase shift modulation of the quasi square-wave voltages generated by their corresponding active-bridge modules.The modulation scheme adopted is the multiple phase shift (MPS),which is an extension of triple phase shift (TPS)[14] used for dual active bridge (DAB). The degrees of freedom are the bridge *i* voltage duty ratios D_i and inter-bridge phase shifts D_{ij} described in Fig.2. These control parameters are obtained using classical phase shifting of gate signals such that $0 \le D_i \le 1$ and $-0.5 \le D_{ij} \le 0.5$ where modulation parameters are normalized with respect to half the switching period. The equivalent fundamental harmonic based representation of the MAB bridge voltages are given by (1), where K_i represents the DC voltage ratio with respect to a reference bridge (*r*). The inclusion of this ratio enables representation of MAB's different operating modes, such that K_i=1 designates unity-gain mode and $K_i \neq 1$ designates buck/boost mode.

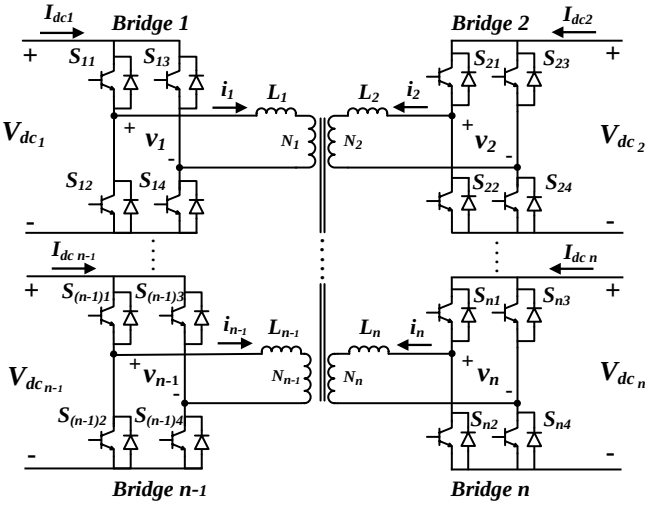

Fig. 1: DC-DC MAB Converter with *n*-ports.

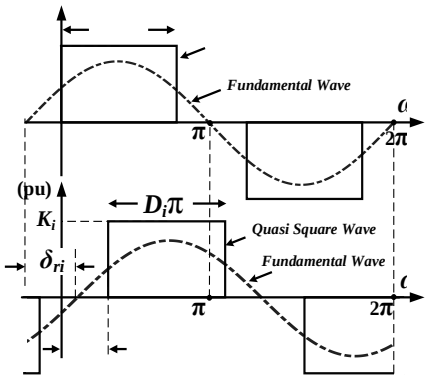

Fig. 2: Illustration of multiple phase shift control in MAB.

$$v_i(t) = V_{i\,max}\,sin\left(\omega t + (1-D_r)\frac{\pi}{2} - \delta_{ri}\right) \quad (1)$$

Such that $v_i(t)$ is bridge i AC per unit voltage and,

$$V_{i\,max} = \frac{4K_i}{\pi} sin\left(\frac{D_i\pi}{2}\right), \boldsymbol{K_i} = \frac{\boldsymbol{N_i V_{dc\,i}}}{\boldsymbol{N_r V_{dc\,r}}}, \delta_{ri} = \pi\left(D_{ri} + \frac{D_i - D_r}{2}\right)$$

Where,
- i=1,2,…,n
- n is total number of ports in MAB
- r is reference bridge, K_r=1, $D_{r\,r}$= $\delta_{r\,r}$= 0
- N_i is transformer number of turns at bridge i
- D_i, D_r and D_{ri} are all defined in Fig.2

B. I-V Characteristics

The definition of the MAB AC current characteristic with respect to the bridge voltages are provided within the section. On the assumption of non-isolated lossless MAB, the I-V characteristics connecting any two active bridges i and j will be considered. Accordingly, the equivalent circuit of the MAB in Fig.1 is depicted in Fig. 3 [24]. The RMS bridge voltages $V_{i_{RMS}}$,and $V_{j_{RMS}}$given by (2) in per unit (for the quasi square waves in Fig. 2) are the independent variables of the proposed I−V characteristic. The dependent variable is $I_{ij_{RMS}}$representing the AC link branch current connecting the two bridges i and j, as shown in Fig. 3. This is outlined in (3), derived using the fundamental harmonic approximation in (1).

$$V_{i_{RMS}} = K_i\sqrt{D_i}\ pu, V_{j_{RMS}} = K_j\sqrt{D_j}\ pu \quad (2)$$

$$I_{ij_{RMS}} = |\overline{I_{ij}}| = \left|\frac{\overline{V_i} - \overline{V_j}}{j\omega L_{ij}}\right|, \quad I_{ij_{RMS}} = -j(\overline{V_i} - \overline{V_j})\ pu \quad (3)$$

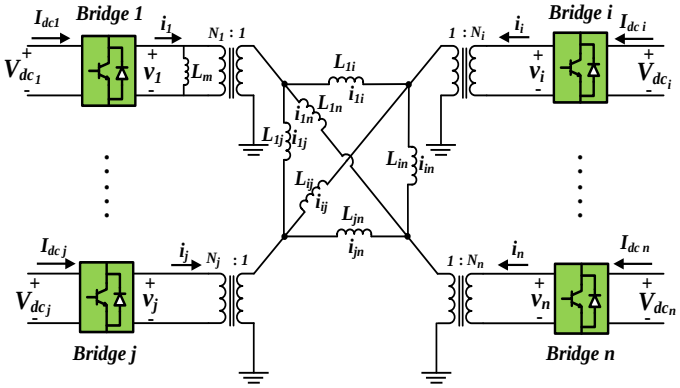

Fig. 3: Equivalent circuit of the MAB converter.

For the ease of analysis, full range of a single independent variable $V_{i_{RMS}}$ is plotted against the dependent variable $I_{ij_{RMS}}$at an arbitrary operating point characterized by P_{ij} and K_{ij} where,

$$P_{ij} = V_{i_{RMS}} V_{j_{RMS}} sin(\delta_{rj} - \delta_{ri})\ pu, \quad K_{ij} = \frac{K_i}{K_j} \quad (4)$$

The arbitrary operating point selected is P_{ij}=0.25pu and K_{ij}=0.5. The output is multiple 2D I-V curves between $I_{ij_{RMS}}$ and $V_{i_{RMS}}$ for several discrete values of $V_{j_{RMS}}$. This is shown in Fig.4(a), where the nonlinear I-V characteristic is clearly presented. It can be noted that some ranges on the curves are void, which means that the relevant RMS voltages do not achieve reference power P_{ij}=0.25pu. To better represent the I-V characteristic at full range of the independent variables ($V_{i_{RMS}}$and $V_{j_{RMS}}$), a 3D representation is developed as shown in Fig.4(b), where $V_{i_{RMS}}$and $V_{j_{RMS}}$are plotted along the horizontal axes, and $I_{ij_{RMS}}$ is plotted along the vertical axis at the same arbitrary operating point (P_{ij}=0.25pu and K_{ij}=0.5). The I−V characteristic curves broadly applies to any AC link branch current I_{ij} in the MAB converter and demonstrates that there is only one specific combination of bridge voltages V_i and V_j that gives the global minimum current for every transferred active power between two bridges P_{ij},. The minimum current point in the AC link branch connecting bridges i and j can be achieved by a unique combination of D_i and D_j at a specific power since $V_{i_{RMS}}$and $V_{j_{RMS}}$are solely dependent on D_i and D_j respectively as revealed from (2). The remaining degrees of freedom are the inter-bridge phase shift angles, which will be used for power flow regulation. Consequently, obtaining a unique global optimal combination of duty ratios (D_1,..D_n) is key to regulate the RMS bridge voltages to track minimum current points in all AC link branches while simultaneously controlling the active power at all ports.

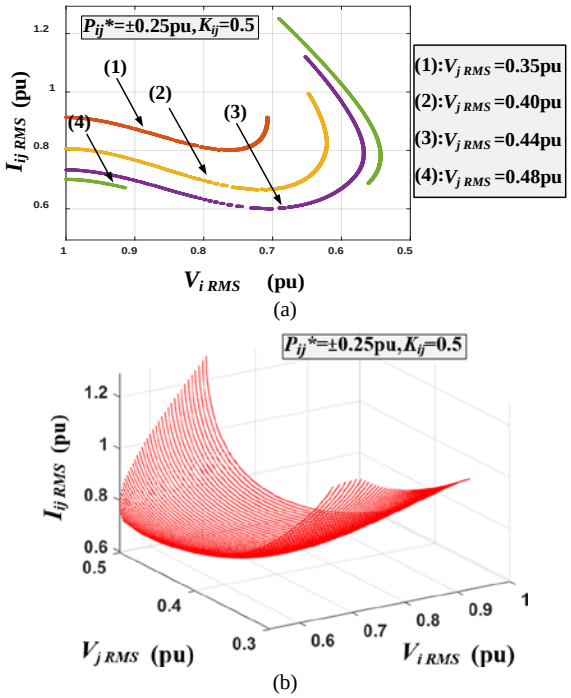

Fig.4: MAB I−V Characteristic at P_{ij}=0.25pu and K_{ij}=0.5 (a) Multiple discrete values of $V_{j\,RMS}$. (b) Full range of $V_{i\,RMS}$ and $V_{j\,RMS}$ in 3D.

III. P&O MCPT Algorithm for MAB Converters

The individual branch currents I_{ij} connecting ports i and j (described in section II-B) are not physically accessible in a practical MAB converter shown in Fig. 1. Instead, the AC port RMS current I_{iRMS} and power P_i will be utilized as these are readily available and can be measured. When I_{iRMS} is minimized, each individual branch current I_{ijRMS} is minimized accordingly, therefore, the I-V characteristic in Fig. 3 is valid for minimization of port current I_{iRMS}. It can be deduced from Fig.3 that for each port i, I_{iRMS} and P_i can be defined by

$$I_{i\,RMS} = \sqrt{\sum_{\substack{j=1 \\ j\neq i}}^{n} (I_{ij\,RMS})^2}\,, \qquad P_i = \sum_{\substack{j=1 \\ j\neq i}}^{n} P_{ij} \tag{5}$$

The search for minimum RMS current point in this I-V characteristic curve follows a so-called 'hill-descent' profile where the initial (and peak) point of this hill corresponds to maximum RMS bridge voltages. The proposed 'hill-descent' P&O-based MCPT is investigated in this section, similar to the hill-climb P&O MPPT [22], [23], on the following basis:

- Perturbing the main control parameter (increment or decrement by a certain step size);
- Monitoring aggregate AC RMS current and active power at DC ports before and after the perturbation;
- Following this, the algorithm would either: keep perturbing in the same direction or perturb in the reverse direction until MCP is realized.

A. Perturbation Parameter

Identifying the main perturbation parameter is vital to allow the application of the hill-descent P&O MCPT algorithm. As the analysis in section II-B has revealed, the perturbation parameter must be restricted to D_i or D_j for the P&O to track minimum RMS current in an AC link branch between ports i and j. Selecting D_i as the P&O perturbation parameter, a mathematical relationship can be derived for its corresponding value of D_j that would ensure minimum current in this AC link branch. Since the global minimum I_{RMS} occurs at equal AC RMS voltages [14]; therefore, equating the two RMS voltages in (2) implies minimum current would flow between any two ports, and hence gives the direct relationship, between the duty ratios.

$$D_j = \left(\frac{K_i}{K_j}\right)^2 D_i \tag{6}$$

Generalising for all AC link branches, this necessitates control of a single bridge RMS voltage only, while all other active bridges would have to maintain and follow the relation in (6). For this sake, bridge 'r' is chosen as the reference, and accordingly D_r will be the main perturbation parameter. In this case, (6) is rewritten as

$$D_i = \begin{cases} \dfrac{D_r}{{K_i}^2} \\ 1, \quad if \ \dfrac{D_r}{{K_i}^2} > 1 \end{cases} \tag{7}$$

Therefore, perturbing D_r while maintaining the relation in (7) to calculate remaining duty ratios will lead to the MCP. Investigation of D_r as a perturbation parameter is provided here for an example Triple Active Bridge (TAB) converter (n=3) to verify the effectiveness of perturbing D_r on minimizing RMS current. To achieve this, a fixed-step perturbation is applied according to the following steps:

1) D_r=1 (maximum RMS voltage of reference bridge).
2) Given DC voltage ratios (K_i) for remaining ports (i=1,..,n and $i\neq r$), calculate remaining duty ratios using (7).
3) For desired port powers (P_1*…P_n*), use power equations (4) and (5) to calculate phase shifts D_{ri}, i=1,..,n and $i\neq r$
4) Calculate aggregate AC link RMS current using:

$$I_{RMS} = \sqrt{\sum_{i=1}^{n} (I_{i\,RMS})^2} \tag{8}$$

5) Calculate new value of D_r (D_r=$D_{r(\text{old})}$−ΔD_r), where ΔD_r is a fixed-step perturb of choice,
6) Repeat steps (2)-(5) and stop when minimum I_{RMS} (MCP) is reached.

Fig. 5 displays the simulation results, where I_{RMS} maintains a 'hill-descent' contour when perturbing D_r (r=1). The results substantiate that selecting a single duty ratio (i.e. duty ratio of reference bridge D_r) as a perturbation parameter leads to minimum current point (MCP), while maintaining the desired power levels at the constant required rate during the perturbation process.

B. Method of Perturb Calculation

The objective of this section is the design of an adaptive-step perturb calculator for MAB converter rather than fixed-step to enhance dynamic performance. The perturb calculator's main objective is to generate large perturb steps at the beginning of the hill-descent to help reach the MCP swiftly, and as moving toward the MCP, reduced perturb step sizes are produced to avoid unnecessary steady-state oscillations across the MCP. On this basis, the proposed adaptive-step perturbs are added or subtracted from the former value of the perturbation parameter D_r based on variations of aggregate AC RMS current I_{RMS} and power P_i. On this basis the PI-based adaptive-step calculator – depicted in Fig. 6, is developed.

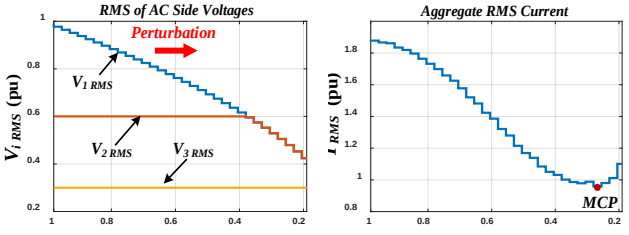

(a)

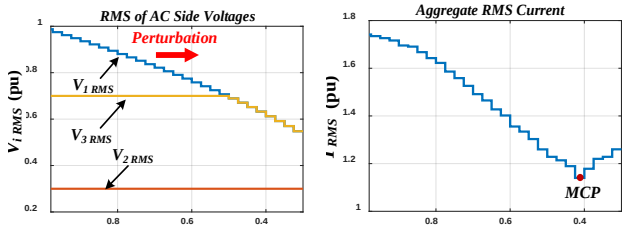

(b)

Fig. 5 : Duty ratio perturbation for TAB converter with (a) K_2 = 0.6, K_3= 0.3 at P_1*= 0.2pu, P_2* = -0.1pu, P_3*=-0.1pu , (b) K_2 = 0.3, K_3= 0.7 at P_1*= 0.15pu, P_2* = 0.1pu, P_3*=-0.25pu

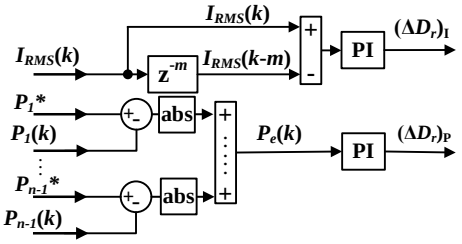

Fig. 6: Proposed adaptive-step PI-based dual-perturb calculator.

The change in I_{RMS} before and after perturbation will be used to calculate adaptive component $(\Delta D_r)_I$. I_{RMS} is outlined by (8) and is defined as the aggregate RMS current of all AC bridges. The change in RMS current will be treated as an error signal that needs to be minimized using conventional PI controller [23]. This will produce $(\Delta D_r)_I$ for tuning the perturbation parameter D_r in order to track minimum current. The change in RMS current is the difference between two consecutive discrete time domain samples within a fixed delay (T_d) of m sampling instants therefore $T_d=m/f_{samp}$, where f_{samp} is the sampling frequency. T_d allows I_{RMS} to reach steady state after perturbation. Note that only (n-1) port powers need regulation, as noticed in Fig.6, as $P_1+P_2+\ldots P_n=0$ and the n^{th} port power will be regulated autonomously to maintain zero net power.

Furthermore, to ensure satisfactory active power regulation, power transfer needs monitoring during the D_r perturbation. This is where the second adaptive component $(\Delta D_r)_P$ is introduced to update D_r in response to difference between the desired active and measured power at all ports as shown in Fig.6. The error signals between the desired and measured port powers, defined as $P_e = \sum_{i=1}^{n-1}|P_i^* - P_i|$, will be treated by a PI controller (after every perturbation) to produce an adaptive perturb $(\Delta D_r)_P$ that minimize this error during perturbation. This will actively decouple the effect of D_r perturbation from the core active power closed loop controller, which will be discussed in section IV. The weight of $(\Delta D_r)_I$ should be higher than $(\Delta D_r)_P$ in the perturbation process given that the key aim of $(\Delta D_1)_P$ is only to fine-tune D_r provided that a separate controller is employed for power regulation. Consequently, the boundaries for the perturb components for arbitrary selection such that $0\leq(\Delta D_r)_I\leq 0.2$pu and $0\leq(\Delta D_r)_P\leq 0.1$pu. Concise functions of the proposed adaptive-step perturbs are as follows:

- **$(\Delta D_r)_I$**: update (correct) D_r in response to the incremental or decremental change of I_{RMS}.
- **$(\Delta D_r)_P$:** fine tune D_r to maintain a close-to-zero error in active power during the perturbation process and to decouple this from the core active power controller.

C. Hill-Descent P&O Algorithm

Starting at D_r=1; the proposed P&O algorithm perturbs D_r while monitoring variation of I_{RMS} and power error P_e. Table I outlines eight operating conditions considering that sign of $(\Delta D_r)_I$ is negative for decremental change in RMS current and is positive for incremental change in RMS current. Careful investigation of Table I revels redundancy in these eight operating conditions; reduction of these conditions into only four conditions is given by (9). Accordingly, Fig.7 illustrates the complete proposed hill-descent P&O algorithm. Monitoring power error must be done within an acceptable value as precise zero tolerance will not facilitate leading to a convergent solution. Therefore, a small tolerance in power error (P_{Tol}=0.005pu) is applied. The proposed hill-descent P&O algorithm involves the following implementation steps:

1. Read $I_{iRMS}(k)$ and power $P_i(k)$from all ports, where k refers to the present sampling instant;
2. Calculate $I_{RMS}(k)$ using (8);
3. Calculate adaptive perturb values $(\Delta D_r)_I$ and $(\Delta D_r)_P$ using perturb calculator in Fig.6.
4. $(\Delta D_r)_I$, $(\Delta D_r)_P$ and $P_e(k)$ in addition to previous values of perturbation parameter $D_r(k\text{-}1)$ and $D_r(k\text{-}m)$ are sent to P&O algorithm which determines $D_r(k)$ according to (9) and as shown in Fig.7.
5. Remaining duty ratios are calculated using (7).
6. Repeat steps (1)-(4).

According to (9), $(\Delta D_r)_P$ is added to $D_r(k)$ to minimize the power error $P_e(k)$, which means that larger $D_r(k)$ lead to smaller $P_e(k)$. In order to clarify this, simulation (assuming P&O is not used) is performed to show the effect of decreasing (perturbing) $D_r(k)$ on $P_e(k)$. When decreasing $D_r(K)$ as shown in Fig 8 (a), phase shifts D_{13} and D_{12} compensate this, in Fig 8(b), to maintain active powers close to reference power levels. This continues until phase shifts saturate (D_{12} reaching upper limit 0.5pu) at t=0.5s as shown in Fig 8 (b), and power error starts to significantly increase as in Fig 8 parts (c) and (d). This explains the need to add a positive $(\Delta D_r)_P$ to $D_r(k)$ to reduce power error.

TABLE I. Operating conditions of proposed P&O Algorithm

	Condition		Action	
1	$I_{RMS}(k)>I_{RMS}(k\text{-}m)$	$D_r(k\text{-}1)>D_r(k\text{-}m)$ &$P_e(k)\leq P_{tol}$	Decrease D_r	$D_r(k)=D_r(k\text{-}m)-(\Delta D_r)_I$
2	$I_{RMS}(k)< I_{RMS}(k\text{-}m)$	$D_r(k\text{-}1)>D_r(k\text{-}m)$ &$P_e(k)\leq P_{tol}$	Increase D_r	$D_r(k)=D_r(k\text{-}m)-(\Delta D_r)_I$
3	$I_{RMS}(k)>I_{RMS}(k\text{-}m)$	$D_r(k\text{-}1)>D_r(k\text{-}m)$ &$P_e(k)>P_{tol}$	-Decrease D_r -Fine tune D_r to minimise P_e	$D_r(k)=D_r(k\text{-}m)-(\Delta D_r)_I$ $+(\Delta D_r)_P$
4	$I_{RMS}(k)< I_{RMS}(k\text{-}m)$	$D_r(k\text{-}1)>D_r(k\text{-}m)$ &$P_e(k)>P_{tol}$	-Increase D_r -Fine tune D_r to minimise P_e	$D_r(k)=D_r(k\text{-}m)-(\Delta D_r)_I$ $+(\Delta D_r)_P$
5	$I_{RMS}(k)>I_{RMS}(k\text{-}m)$	$D_r(k\text{-}1)<D_r(k\text{-}m)$ &$P_e(k)\leq P_{tol}$	Increase D_r	$D_r(k)=D_r(k\text{-}m)+(\Delta D_r)_I$
6	$I_{RMS}(k)< I_{RMS}(k\text{-}m)$	$D_r(k\text{-}1)<D_r(k\text{-}m)$ &$P_e(k)\leq P_{tol}$	Decrease D_r	$D_r(k)=D_r(k\text{-}m)+(\Delta D_r)_I$
7	$I_{RMS}(k)>I_{RMS}(k\text{-}m)$	$D_r(k\text{-}1)<D_r(k\text{-}m)$ &$P_e(k)>P_{tol}$	-Increase D_r -Fine tune D_r to minimise P_e	$D_r(k)=D_r(k\text{-}m)+(\Delta D_r)_I$ $+(\Delta D_r)_P$
8	$I_{RMS}(k)< I_{RMS}(k\text{-}m)$	$D_r(k\text{-}1)<D_r(k\text{-}m)$ &$P_e(k)>P_{tol}$	-Decrease D_r -Fine tune D_r to minimise P_e	$D_r(k)=D_r(k\text{-}m)+(\Delta D_r)_I$ $+(\Delta D_r)_P$

$$D_r(k)=\begin{cases} D_r(k-m)+(\Delta D_r)_I, & [P_e(k)\leq P_{Tol} \text{ AND } D_r(k-1)<D_r(k-m)] \\ D_r(k-m)-(\Delta D_r)_I, & [P_e(k)\leq P_{Tol} \text{ AND } D_r(k-1)>D_r(k-m)] \\ D_r(k-m)+(\Delta D_r)_I+(\Delta D_r)_P, & [P_e(k)>P_{Tol} \text{ AND } D_r(k-1)<D_r(k-m)] \\ D_r(k-m)-(\Delta D_r)_I+(\Delta D_r)_P, & [P_e(k)>P_{Tol} \text{ AND } D_r(k-1)>D_r(k-m)] \end{cases} \quad (9)$$

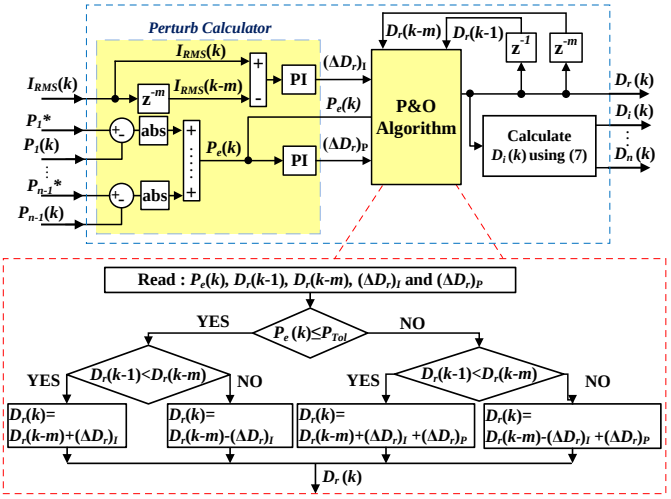

Fig. 7: MCPT algorithm incorporating the adaptive-step PI-based dual-perturb calculator and Hill-Descent Perturb and Observe algorithm and.

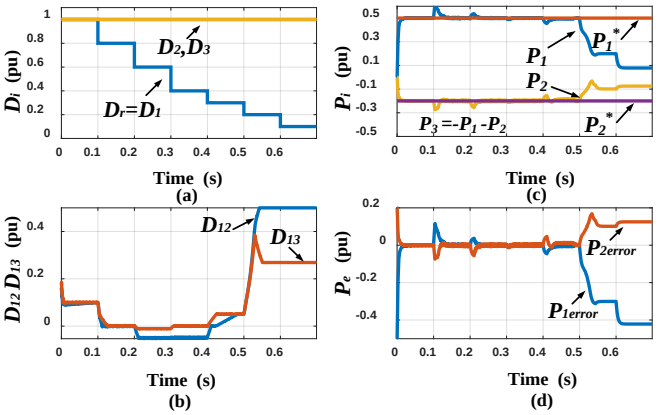

Fig 8: Effect of decreasing D_r on active Power (without P&O) at K_{12}=0.6, K_{13}=0.4, P_1*=0.5pu and P_2*=-0.2pu: (a) Pertrubation parameter D_r. (b) Phase Shifts D_{12} and D_{13}. (c)Transferred Power (Note: P_3=- P_1-P_2). (e) Power error.

IV. Complete Power Flow Controller Design

The P&O MCPT algorithm developed so far can only generate local duty ratios (D_i…..D_n) for the quasi square wave voltage outputs of the individual bridges. Power flow regulation has not been addressed yet, as the main control variables realizing this are the inter-bridge phase shifts (D_{ri}……D_{rn}). The relationship between these inter-bridge phase shifts and the corresponding power flows is nonlinear and highly coupled. Therefore, in this section, a new phase shift decoupler is derived to facilitate power flow regulation. The design of the complete controller, including both phase shift decoupler and P&O MCPT algorithm, is finally presented.

A. Phase Shift Decoupler

The aim of this subsection is to develop a simple and scalable phase shift decoupler for MAB converter with any number of ports. The coupled nonlinear relationship of phase shifts with power at each bridge makes it vital to develop a phase shift decoupler to enable utilizing conventional PI controllers for power flow regulation. This nonlinear steady state equation for port i power (P_i) is derived from (4) and (5) using superposition method and assuming unity gain mode at all ports (K_1=…=K_n=1) and full square wave voltages at the bridges (D_1=…=D_n=1) to simplify analysis in terms of inter-bridge phase shifts only (D_{ri}……D_{rn})

$$P_i = \frac{1}{n}\left[\sum_{j=1}^{n} \mathrm{Sin}\,\pi(D_{ri} - D_{rj})\right], i = 1,2,\ldots\ldots,n \qquad (10)$$

A general linearized form of the power flow characteristics can be deduced as outlined by (11) by applying Taylor's series to (10)around equilibrium points$a_i = D_{ri} = 0$, for $i = 1,2,\ldots\ldots,n$

$$P_i = \sum_{j=1}^{n}\left[\frac{\partial P_i}{\partial D_{rj}}(a_1 \ldots a_n)\right] D_{rj}\ , i = 1,2,\ldots\ldots,n \qquad (11)$$

Accordingly, (11) can be re-written as follows:

$$\begin{bmatrix} P_1 \\ \vdots \\ P_n \end{bmatrix} = \begin{bmatrix} \frac{\partial P_1}{\partial D_{r1}} & \cdots & \frac{\partial P_1}{\partial D_{rn}} \\ \vdots & \ddots & \vdots \\ \frac{\partial P_n}{\partial D_{r1}} & \cdots & \frac{\partial P_n}{\partial D_{rn}} \end{bmatrix} \begin{bmatrix} D_{r1} \\ \vdots \\ D_{rn} \end{bmatrix} \qquad (12)$$

Re-arranging (12) yields

$$\begin{bmatrix} D_{r1} \\ \vdots \\ D_{rn} \end{bmatrix} = \begin{bmatrix} \frac{\partial P_1}{\partial D_{r1}} & \cdots & \frac{\partial P_1}{\partial D_{rn}} \\ \vdots & \ddots & \vdots \\ \frac{\partial P_n}{\partial D_{r1}} & \cdots & \frac{\partial P_n}{\partial D_{rn}} \end{bmatrix}^{-1} \begin{bmatrix} P_1 \\ \vdots \\ P_n \end{bmatrix} = \begin{bmatrix} A_{11} & \cdots & A_{1n} \\ \vdots & \ddots & \vdots \\ A_{n1} & \cdots & A_{nn} \end{bmatrix} \begin{bmatrix} P_1 \\ \vdots \\ P_n \end{bmatrix} \qquad (13)$$

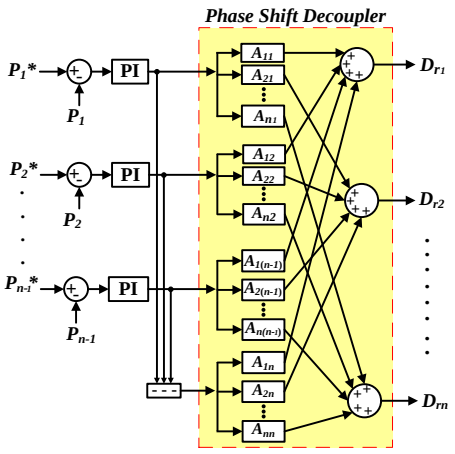

Fig. 9: PI-based phase shift decoupling controller for MAB converter.

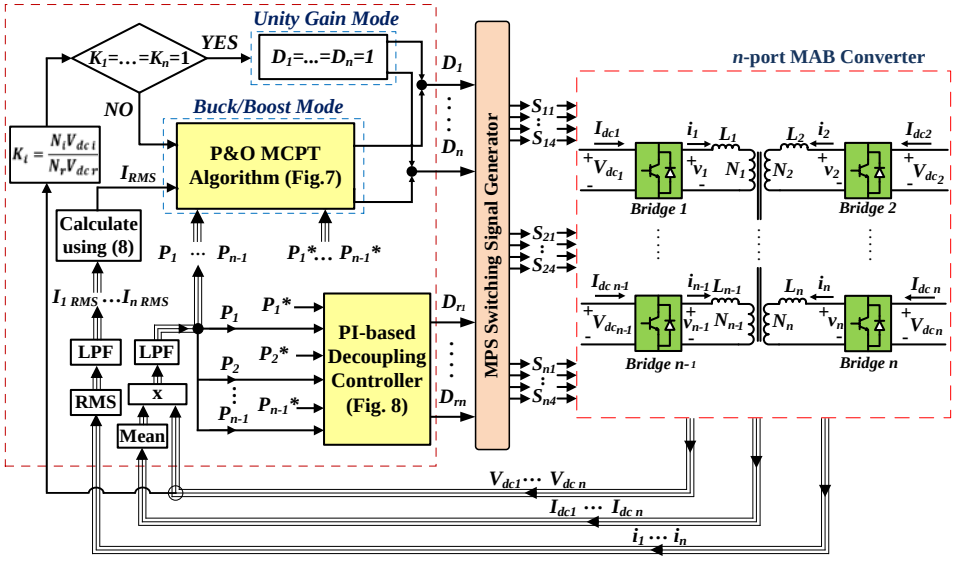

Fig. 10: Proposed MCPT power flow controller for DC-DC MAB converter.

However, for power flow control, only (n-1) port powers need to be regulated, as the n^{th} port power is regulated autonomously to maintain net zero power. A decoupling controller is developed based on (13) as shown in Fig. 9 where the open loop port powers P_i in (13)are replaced by a closed loop regulator of power, where conventional PI controllers are deployed to regulate the power error (P_i*-P_i) for each port. Port powers for (n-1) ports only are regulated and the port power for n^{th} port is derived autonomously based on

$$P_n = -\sum_{j=1}^{n-1} P_j \tag{14}$$

The outcome is a scalable power flow controller that is applicable to MAB converter with any number of ports. It should be mentioned that the selection of the port where power is autonomously (not directly) regulated is based on the port most likely to operate with least DC side current I_{dc}. This is to save adding a current transducer to measure I_{dc} at this port where it may be most prone to pick up measurement noise leading to unsatisfactory dynamic response.

B. Integrated Controller Structure

The P&O MCPT algorithm (section III) and the PI-based phase shift decoupler (section IV-A) are integrated to realize the complete 'MCPT power flow' controller as shown in Fig.10. The phase shift decoupler performs power flow control, while the MCPT algorithm produces optimal duty ratios to realize minimum aggregate AC RMS current. The controller is generalized for n-ports MAB DC-DC converter regardless of power and voltage ratings. In addition, it incorporates all possible operating modes; Buck/boost (K_1≠1and/or K_2≠1…K_n≠1) and unity gain (K_1=…=K_n=1). In unity gain mode the MCPT technique will not be applied as the minimum current is obtained at unity duty ratios (D_1=…=D_n=1) in this case [14]. On the other hand, in buck/boost operating mode; the MCPT technique is utilized to generate optimal duty ratios (D_1…D_n). Inter-bridge phase shifts (D_{ri}...D_{rn}) are obtained via the PI-based phase shift decoupler in order to regulate power flow. This can be implemented via the following steps:

1) Read measured DC voltages (V_{dc1}… V_{dcn}) and currents (I_{dc1}… $I_{dc\,n}$). Calculate port powers (P_1… P_{n-1});
2) Phase shift decoupler regulates port powers (P_1…P_{n-1}) against desired power levels (P_1*… P_{n-1}*) to generate inter-bridge phase shifts (D_{r1}...D_{rn});
3) Read AC currents (i_1… i_n) and calculate aggregate RMS current I_{RMS};
4) Calculate the DC voltage ratios (K_1….K_n):
   a.For Buck/boost modes (K_1≠1and/or…K_n≠1): apply MCPT algorithm (i.e.: perturb calculation and P&O algorithm depicted in Fig. 7) to generateD_1….D_n.
   b. For unity gain mode (K_1…K_n=1); duty ratios are directly generated D_1=…=D_n=1;
5) Inter-bridge phase shifts and duty ratios from steps 2 and 4 are then sent to multiple phase shift (MPS)switching signal generator.
6) Repeat steps 1-5.

V. Simulation and Experimental Validation

This section presents validation of the proposed controller in Fig.10. Both simulation and experimental results are provided for a Triple Active Bridge (TAB) converter. The simulations and experiments were carried out using the MAB circuit parameters in Table II, which refers to the circuit diagram in Fig.1.

TABLE II. Parameters of Converter

Parameter	value
DC Voltage of Bridge 1 V_{dc1}	100V
DC Voltage of Bridge 2 V_{dc2}	K_2*100V
DC Voltage of Bridge 3 V_{dc3}	K_3*100V
Switching Frequency f_s	2.5kHz
Turns ratio N_1: N_2: N_3	1:1:1
Leakage Inductances L_1,L_2,L_3	0.21mH
Maximum Power P_{max}	1638W

A. Simulation Results

Simulation model of the proposed controller in Fig.10 is built in MATLAB/Simulink, for TAB converter and results are presented for two test scenarios in Fig.11.The controller satisfies the required P* at bridges 1,2 and 3 with negligible oscillations as shown in Fig.11(c). The aggregate AC RMS current, outlined by (8), is shown in Fig.11 (d). The RMS currents are benchmarked against minimum RMS current (calculated offline) to verify that minimum current is achieved by the proposed controller. The offline methodology to calculate the minimum I_{RMS} utilizes (1)-(5) to iteratively scan through the entire range of phase ratios that achieve the reference powers and record the minimum I_{RMS} that satisfies those powers. For the test scenarios in Fig.11, it was found out that these powers can be achieved where $1.39A \leq I_{RMS} \leq 1.71A$ and $1.25A \leq I_{RMS} \leq 1.65A$ respectively, with the proposed controller successfully achieving the minimum value in both cases. After the initiation point of perturbation at D_1=…=D_n=1, RMS current starts to decrease as the MCPT algorithm approaches the optimal modulation parameters achieving negligible oscillation at steady state. It can be seen from Fig.11 (c) that active power profile is different than RMS current minimization profile in Fig 11 (d), as the power reaches steady state very shortly after 5 cycles. RMS current minimization profile reflects number of perturbations and depends on many factors including boundaries of perturb components – full evaluation of controller performance is discussed later in section VI. The ripples in the power waveforms in 0<t<0.3 and 0.6<t<0.9 are due to the continued perturbation of duty ratios (D_1, D_2, D_3) – as shown in Fig 11(a), until MCP is reached. This causes the phase shift decoupler to update the inter-bridge phase shifts (D_{12}, D_{13}, D_{23}) – as shown in Fig 11(b), to continuously maintain the required power levels (P_1^*, P_2^*, P_3^*).

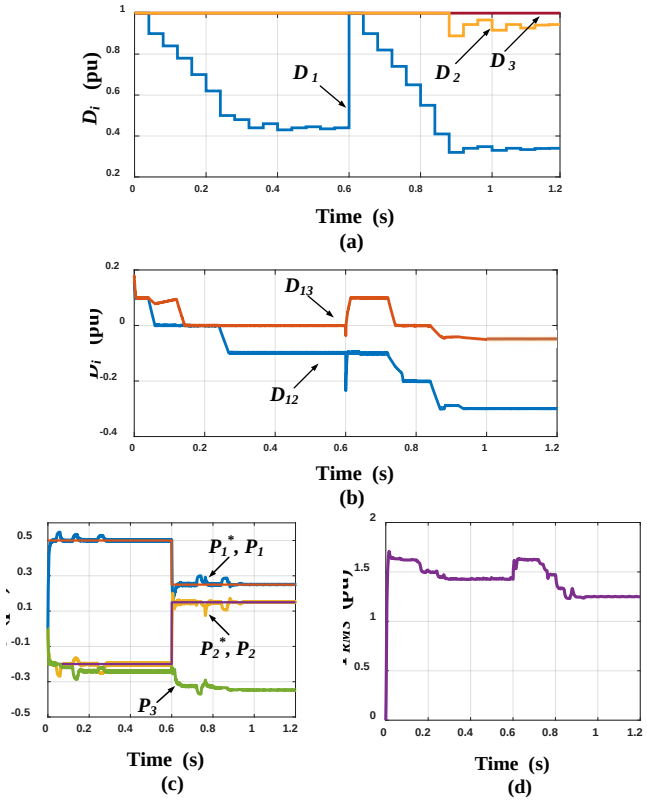

Fig 11: Dynamic Perfromance of Triple Active Bridge Converter Under Proposed MCPT Controller with Step Change at K_{12}=0.6, K_{13}=0.4, P_1*=0.5 to 0.25 pu and P_2*=-0.2 to 0.15 pu: (a) Duty ratios including Pertrubation parameter D_1. (b) Phase Shifts D_{12} and D_{13}. (c) Transferred Power. (d) Aggregate AC RMS current.

B. Experimental Results

A low scaled experimental TAB setup is shown in Fig.12 to verify the performance of the proposed controller depicted in Fig.10 The parameters used for the test rig implementation are listed in Table II. Three programmable DC power supplies are used with shunt resistors to sink power. MOSFETs IRF250 are utilized as the semiconductor switches while the utilized microcontroller is CY8C5888LTI-LP097 PSoC 5LP. The currents and voltages are fedback to the microcontroller using LEM LA55-P and LEM LV25-P hall-effect transducers.

The experimental results in Fig.13 and Fig.14 demonstrate a steady state performance comparison between the proposed controller and phase-shifted control [1], [11] at two operating points. The AC voltages (v_1, v_2, v_3, i_1, i_2, i_3) in addition to the AC RMS current readings are show in Figs 13 & 14. Calculated aggregate RMS current I_{RMS} (A) are shown (at bottom of Figs 13 and 14) as performance indicator. The I_{RMS} with and without the proposed technique clearly demonstrates the effectiveness of the controller. In test scenarios of Figs.13 and 14; power levels can be achieved such that 10.36A≤ I_{RMS} ≤ 12.89A and 9.81A≤ I_{RMS} ≤12.76A respectively. The relative deviation between experimental I_{RMS} (with the proposed controller) and the benchmark minimum values are 2.64% and 3.24% in test scenarios shown in Figs 13(b) & 14(b) respectively. The deviation is mainly due to component parasitics and real time measurements affected by noise and measurement errors. This confirms the effectiveness of the proposed controller in experiment. Note that the benchmark minimum I_{RMS} are iteratively calculated offline utilizing the same procedure mentioned in section V-A.

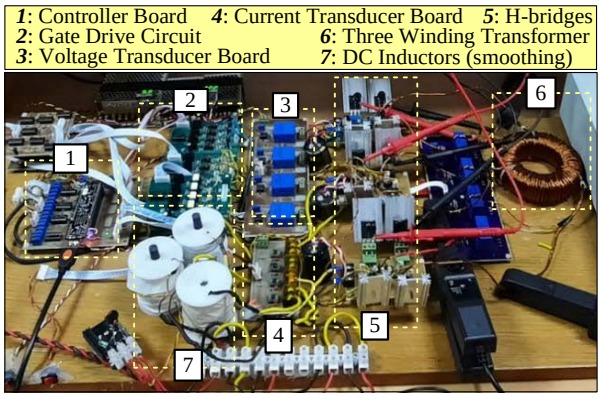

Fig. 12: Experimental test rig for TAB converter.

In order to demonstrate system dynamics under proposed scheme, the full profile of experimental RMS currents is depicted in Fig 15 for Triple active bridge corresponding to test scenario (in Fig 13) at K_2=0.6 & K_3=0.4, P_1*=0.5pu (408W), P_2*=-0.2pu (-164W), P_3=-0.3pu (-244W). Furthermore, to illustrate the experimental performance of controller at step load change, Fig 16 show active powers P_1, P_2 *and* P_3 (P_3=-P_1-P_2) calculated from experimental DC currents and DC voltages at ports 1, 2 and 3. After load change, proposed MCPT controller resets and instantaneously achieves active powers.

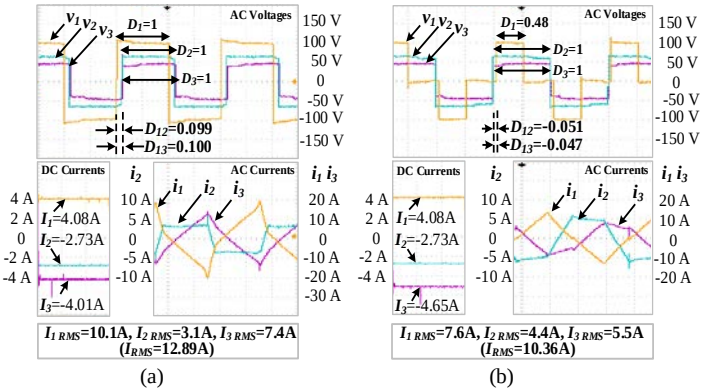

Fig. 13: Steady state experimental performance of TAB Converter under proposed controller with K_2=0.6 & K_3=0.4, P_1*=0.5pu (408W), P_2*=-0.2pu (-164W), P_3=-0.3pu (-244W): (a)Without proposed P&O controller[1], [11] (b) With proposed P&O controller.

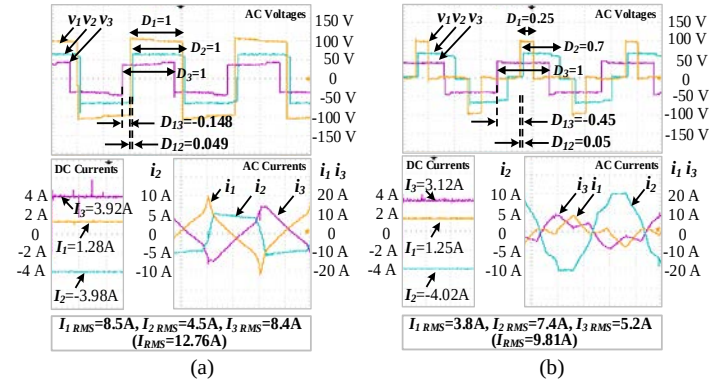

Fig. 14: Steady state experimental performance of TAB Converter under proposed controller with K_2=0.6 & K_3=0.4, P_1*=0.15pu(123W), P_2*=-0.3pu (-245W), P_3=0.15pu (122W): (a)Without proposed P&O controller[1], [11] (b) With proposed P&O controller.

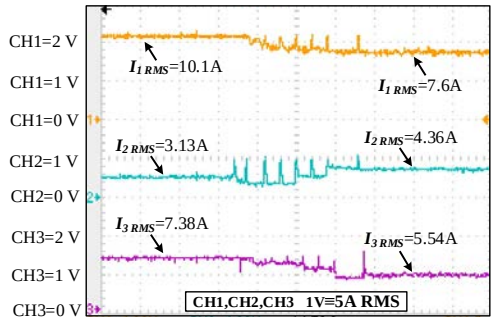

Fig 15: Full experimental RMS current profile in triple active bridge under proposed controller at K_2=0.6 & K_3=0.4, P_1*=0.5pu(408W), P_2*=-0.2pu (-164W), P_3=-0.3pu(-244W) – corresponding to Fig 13.

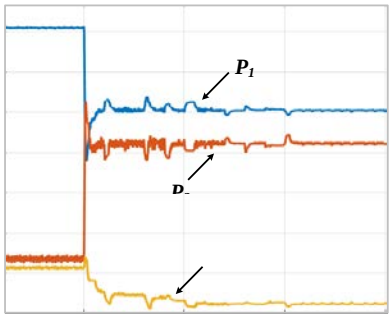

Fig 16: DC Powers calculated from Experimental rig for triple active bridge under proposed controller at K_2=0.6 & K_3=0.4 with load change from P_1*=0.5pu(408W) to 0.25 pu(204) and P_2*=-0.2pu(-164W) to 0.15 pu(122W).

VI. Controller Performance Evaluation

In this section, full evaluation of the proposed controller performance is provided. Evaluation is divided into three main aspects:

a) Accuracy in power flow control – is high with a negligible power error of $|P_e|\leq 0.005$pu at steady state, and an instantaneous power error during perturbation where $|P_e|\leq 0.053$pu as shown in Fig 17 such that $(P_e)_i = P_i^* - P_i$.

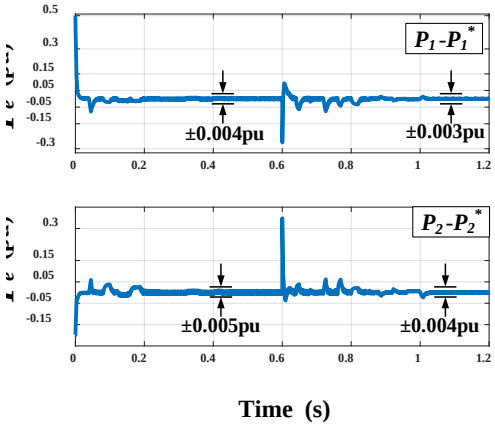

Fig 17: Error in power transfer in Triple Active Bridge Converter Under Proposed MCPT Controller with Step Change at K_2=0.6, K_3=0.4, P_1*=0.5 to 0.25 pu and P_2*=-0.2 to 0.15 pu.

b) Accuracy in achieving global minimum RMS currents – is high as discussed in section V (A,B).

c) Time cost – is sufficient compared to phase-shifted control [1], [11] such that the proposed controller achieves desired power with a rise time t_r of 5 cycles (at 2500Hz) as shown in Fig 18.

For further verification of the effectiveness of the controller, comparative efficiency curves are shown in Fig 19 for a TAB converter between control schemes in [11], [12] and the proposed controller. The efficiency is presented at all per unit power levels at bridge 1 and equally distributed power at bridges 2 and 3 (P_2=P_3=-0.5P_1) with non-unity voltage gains being K_2=0.4 & K_3=0.6. Advantages of the proposed scheme in comparison with other existing control schemes are summarised in Table III.

Other aspects of technical evaluation for the proposed scheme are as follows:

a) Compared to conventional control schemes, the only additional sensor needed for the proposed controller (per bridge) is the ac-side current sensor. Taking into consideration the advantages of the proposed controller (described in Table III) the cost of the additional sensor would be justified.

b) Full ZVS operation is not guaranteed such that under proposed control scheme two bridges of a TAB converter operate in ZVS while the third bridge might lose ZVS operation. Fig 20 shows the region of partial ZVS (ZVS in two bridges) against minimum current points achieved under proposed controller in a TAB converter over the entire power range and non-unity DC voltage mismatch.

c) The minimum RMS current is not achieved with similar profile compared to power flow control. This specifically occurs when the optimal D's are far from initiation point D_1=…=D_n=1 (at light load and high DC voltage ratios). This also depends on the boundaries of perturb components $(\Delta D_r)_P$ & $(\Delta D_r)_I$. Increasing these boundaries would rapid up RMS current minimization but will cause series steady state oscillations. However, the RMS

Table III: Advantages of the proposed scheme in comparison with other existing control schemes.

Criteria \ Reference	[1]	[7]	[11]	[12]	Proposed Scheme
Controller Complexity (Amount of offline calculations, Modelling & optimization complexity…etc)	Medium	High	Medium	Medium	Low
Controller Dependency on converter modelling	Yes	Yes	Yes	Yes	No
Controller Robustness to System Parameters Variation	No	No	No	No	Yes
Controller Independence of Bridge Topologies (half-bridge, full-bridge, multi-level….etc).	No	No	No	No	Yes
Controller Applicability for N-port MAB Converters	No	Yes	No	No	Yes
Controller Dependency on Look-up Table for Implementation	Yes	Yes	No	No	No
Conversion Efficiency in MAB converter	Medium	Low	Medium	Low	High

current profile does not affect the performance of the proposed controller in power flow regulation in terms of instantaneous control requirement and steady state power error – as discussed above. This is thanks to the adaptive perturb $(\Delta D_r)_P$ that minimize the power error during perturbation, hence actively decouple the effect of D_r perturbation from the embedded power controller (Fig 9).

VII. Conclusion

A new power regulation controller − incorporating a novel scheme that tracks minimum RMS current to minimize conductive losses, has been proposed for multi active bridge (MAB) DC−DC converter. The existence of a global minimum current for every transferred active power level between the DC ports were established from the MAB I-V characteristic. The proposed P&O algorithm tracks minimum current point and is combined with a closed loop phase shift decoupler for active power regulation. Unlike existing efforts in this field, the proposed controller is universal, independent of circuit parameters. In addition, the controller design does not prerequisite cumbersome converter modelling. The effectiveness and potential of the proposed controller were verified through simulations and an experimental test rig.

References

[1] C. Zhao, S. D. Round, and J. W. Kolar, "An isolated three-port bidirectional dc-dc converter with decoupled power flow management," *IEEE Trans. Power Electron.*, vol. 23, no. 5, pp. 2443–2453, 2008.

[2] V. N. S. R. Jakka, A. Shukla, and G. D. Demetriades, "Dual-Transformer-Based Asymmetrical Triple-Port Active Bridge (DT-ATAB) Isolated DC-DC Converter," *IEEE Trans. Ind. Electron.*, vol. 64, no. 6, pp. 4549–4560, 2017.

[3] C. Gu, Z. Zheng, L. Xu, K. Wang, and Y. Li, "Modeling and Control of a Multiport Power Electronic Transformer (PET) for Electric Traction Applications," *IEEE Trans. Power Electron.*, vol. 31, no. 2, pp. 915–927, 2016.

[4] S. Falcones, R. Ayyanar, and X. Mao, "A DC-DC Multiport-converter-based solid-state transformer integrating distributed generation and storage," *IEEE Trans. Power Electron.*, vol. 28, no. 5, pp. 2192–2203, 2013.

[5] G. Buticchi, L. F. Costa, D. Barater, M. Liserre, and E. D. Amarillo, "A Quadruple Active Bridge Converter for the Storage Integration on the More Electric Aircraft," *IEEE Trans. Power Electron.*, vol. 33, no. 9, pp. 8174–8186, 2018.

[6] H. Tao, A. Kotsopoulos, J. L. Duarte, and M. A. M. Hendrix, "Family of multiport bidirectional DC–DC converters," *IEE Proc-Electro. Power Appl.*, vol. 153, pp. 978–982, 2006.

[7] B. J. D. Vermulst, J. L. Duarte, E. A. Lomonova, and K. G. E. Wijnands, "Scalable multi-port active-bridge converters: modelling and optimised control," *IET Power Electron.*, vol. 10, no. 1, pp. 80–91, 2017.

[8] Z. Guo, "Modulation Scheme of Dual Active Bridge Converter for Seamless Transitions in Multiworking Modes Compromising ZVS and Conduction Loss," *IEEE Trans. Ind. Electron.*, vol. 67, no. 9, pp. 7399–7409, 2020.

[9] L. F. Costa, F. Hoffmann, G. Buticchi, and M. Liserre, "Comparative Analysis of Multiple Active Bridge Converters Configurations in Modular Smart Transformer," *IEEE Trans. Ind. Electron.*, vol. 66, no. 1, pp. 191–202, 2019.

[10] J. Liu *et al.*, "Voltage Balance Control Based on Dual Active Bridge DC / DC Converters in a Power Electronic," *IEEE Trans. POWER Electron.*, vol. 33, no. 2, pp. 1696–1714, 2018.

[11] Y. Chen, P. Wang, H. Li, and M. Chen, "Power flow control in multi-Active-bridge converters: Theories and applications," in *Conference Proceedings - IEEE Applied Power Electronics Conference and Exposition - APEC*, 2019, vol. 2019-March, pp. 1500–1507.

[12] M. Rashidi, N. N. Altin, S. S. Ozdemir, A. Bani-Ahmed, and A. Nasiri, "Design and Development of a High-Frequency Multiport Solid-State Transformer with Decoupled Control Scheme," *IEEE Trans. Ind. Appl.*, vol. 55, no. 6, pp. 7515–7526, 2019.

[13] N. Hou, W. Song, and M. Wu, "Minimum-Current-Stress Scheme of Dual Active Bridge DC-DC Converter with Unified Phase-Shift Control," *IEEE Trans. Power Electron.*, vol. 31, no. 12, pp. 8552–8561, 2016.

[14] O. M. Hebala, A. A. Aboushady, K. H. Ahmed, and I. Abdelsalam, "Generic Closed-Loop Controller for Power Regulation in Dual Active Bridge DC-DC Converter With Current Stress Minimization," *IEEE Trans. Ind. Electron.*, vol. 66, no. 6, pp. 4468–4478, 2019.

[15] F. Krismer and J. W. Kolar, "Closed form solution for minimum conduction loss modulation of DAB converters," *IEEE Trans. Power Electron.*, vol. 27, no. 1, pp. 174–188, 2012.

[16] H. Shi, H. Wen, Y. Hu, and L. Jiang, "Reactive Power Minimization in Bidirectional DC-DC Converters Using a Unified-Phasor-Based Particle Swarm Optimization," *IEEE Trans. Power Electron.*, vol. 33, no. 12, pp. 10990–11006, 2018.

[17] S. Inoue and H. Akagi, "A bidirectional DC-DC converter for an energy storage system with galvanic isolation," *IEEE Trans. Power Electron.*, vol. 22, no. 6, pp. 2299–2306, 2007.

[18] M. Kim, M. Rosekeit, S. K. Sul, and R. W. A. A. De Doncker, "A dual-phase-shift control strategy for dual-active-bridge DC-DC converter in wide voltage range," *8th Int. Conf. Power*

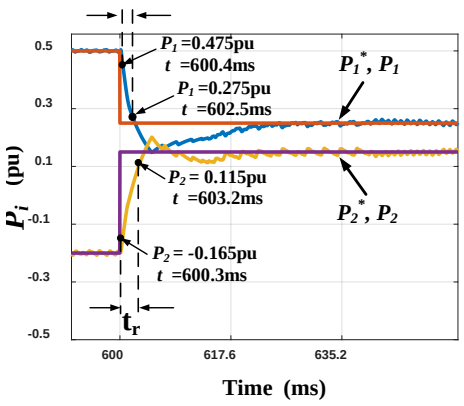

Fig 18: Rise time of acitve powers in Triple Active Bridge Converter Under Proposed MCPT Controller at Step Change with K_2=0.6, K_3=0.4, P_1*=0.5 to 0.25 pu and P_2*=-0.2 to 0.15 pu.

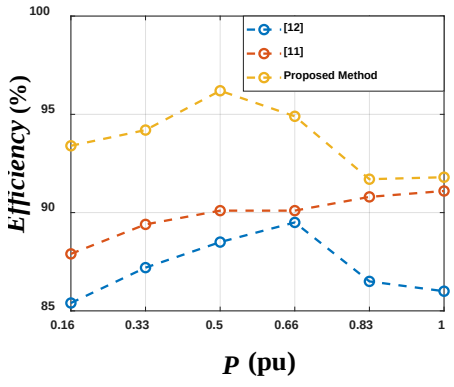

Fig 19: Efficiency curves in TAB converter using control schemes in [11], [12] and the proposed controller at all power levels of P_1 and equally distributed power of P_2 and P_3 with K_2=0.4 & K_3=0.6.

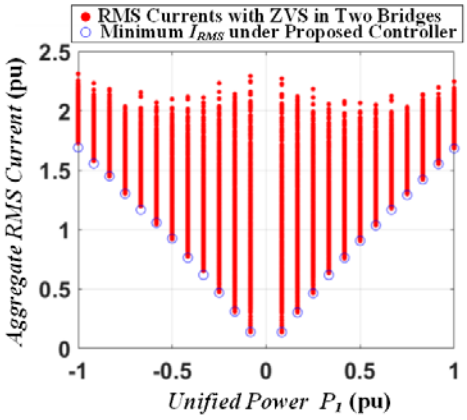

Fig 20: Region of partial ZVS (ZVS in two bridges) against minimum current points achieved under the proposed controller in a triple active bridge (TAB) converter with P_2=P_3=-0.5P_1, K_2=0.4 & K_3=0.6.

Electron. - ECCE Asia "Green World with Power Electron. ICPE 2011-ECCE Asia, pp. 364–371, 2011.

[19] B. N. Alajmi, K. H. Ahmed, S. J. Finney, and B. W. Williams, "A Maximum Power Point Tracking Technique for Partially Shaded Photovoltaic Systems in Microgrids," vol. 60, no. 4, pp. 1596–1606, 2013.

[20] M. Fortunato, A. Giustiniani, G. Petrone, G. Spagnuolo, and M. Vitelli, "Maximum Power Point Tracking in a Photovoltaic Inverter," *IEEE Trans. Ind. Electron.*, vol. 55, no. 7, pp. 2684–2693, 2008.

[21] S. Park, G. Cha, Y. Jung, C. Won, and S. Member, "Design and Application for PV Generation System Using a Soft-Switching Boost Converter With SARC," *IEEE Trans. Ind. Electron.*, vol. 57, no. 2, pp. 515–522, 2010.

[22] M. A. Elgendy, B. Zahawi, and D. J. Atkinson, "Assessment of perturb and observe MPPT algorithm implementation techniques for PV pumping applications," *IEEE Trans. Sustain. Energy*, vol. 3, no. 1, pp. 21–33, 2012.

[23] A. K. Abdelsalam, A. M. Massoud, S. Ahmed, and P. N. Enjeti, "High-performance adaptive Perturb and observe MPPT technique for photovoltaic-based microgrids," *IEEE Trans. Power Electron.*, vol. 26, no. 4, pp. 1010–1021, 2011.

[24] A. J. Hanson and D. J. Perreault, "Modeling the Magnetic Behavior of N-Winding Components: Approaches for Unshackling Switching Superheroes," *IEEE Power Electron. Mag.*, vol. 7, no. 1, pp. 35–45, 2020.

Osama M. Hebala received the B.Sc. (Hons.) and M.Sc. degrees in Electrical and Control Engineering from Arab Academy for Science, Technology & Maritime Transport (AASTMT), Alexandria, Egypt, in 2011 and 2015, respectively. He received the Ph.D. degree in power electronics from Robert Gordon University, Aberdeen, UK, 2020. Currently he is a lecturer in Electric & Control Engineering department at Arab Academy for Science, Technology and Maritime Transport, Alexandria, Egypt. His research interests include DC–DC converters, power conversion systems, and power systems planning and optimization.

Ahmed A. Aboushady (M'04, SM'17) received his BSc (Hons) and MSc degrees in Electrical and Control Engineering from the Arab Academy for Science and Technology, Egypt in 2005 and 2008 respectively. Following this, he obtained his PhD degree in power electronics form the University of Strathclyde, UK in 2013. He is currently a Senior Lecturer in power electronic systems at Glasgow Caledonian University, UK. Dr Aboushady has several publications in refereed journals/conferences as well as a published textbook, a book chapter contribution and a PCT patent No. PCT/GB2017/051364. His research interests are DC/DC converters, high voltage DC transmission systems, grid integration of renewable energy and distributed generation systems.

Khaled H. Ahmed (M'09, SM'12) received the B.Sc. (Hons.) and M.Sc. degrees from Alexandria University, Egypt in 2002 and 2004, respectively. He received the Ph.D. degree in power electronics applications from the University of Strathclyde, UK, 2008. He was appointed as a Professor at Alexandria University, Egypt since 2019. Currently, Dr Ahmed is a Reader in Power Electronics at the University of Strathclyde, UK. He is a senior member of the IEEE Power Electronics and Industrial Electronics societies. Dr Ahmed has published more than 120 technical papers in refereed journals and conferences as well as a published textbook entitled 'High Voltage Direct Current Transmission: Converters, Systems and DC Grids', a book chapter contribution, and a PCT patent PCT/GB2017/051364. His research interests are renewable energy integration, high power converters, offshore wind energy, DC/DC converters, HVDC, and smart grids.

Ibrahim Abdelsalam received a first class B.Sc. and M.Sc. degrees in Electrical Engineering from the Arab Academy for Science and Technology and Maritime Transport (AASTMT), Egypt, in 2006(Alexandria campus) and 2009(Cairo campus). He received the Ph.D. degree in power electronics from University of Strathclyde, Glasgow, UK, 2016. Currently he is a lecturer in Electrical Engineering Department at Arab Academy for Science, Technology and Maritime Transport, Cairo, Egypt. His research interests are power electronic converters and their applications in wind energy conversion systems, and advanced control strategies of the multilevel voltage and current source converters.